JOURNAL OF AIRCRAFT
Vol. 43, No. 1, January–February 2006

Noise-Minimum Runway-Independent Aircraft Approach Design for Baltimore–Washington International Airport

Min Xue* and Ella M. Atkins†
University of Maryland, College Park, Maryland 20742

Vertical or short takeoff and landing aircraft can increase passenger throughput at major urban airports via the use of vertiports or stub runways. The concept of simultaneous noninterfering operations has been proposed to reduce traffic delays by creating approach and departure corridors that do not intersect existing fixed-wing routes. This paper introduces an optimization technique for segmented three-dimensional simultaneous noninterfering trajectory design based on an incremental search strategy that combines a *k*-ary tree with Dijkstra's algorithm. Existing fixed-wing traffic corridors are modeled as impenetrable obstacles. The objective function is based on a validated AH-1 rotorcraft noise model as well as terminal area population density data. Flight envelope limits are represented as search-space constraints. Candidate final approach trajectories for Baltimore–Washington International (BWI) Airport are presented, illustrating the effects of population density, entry region, and varied number of trajectory segments on the optimal result. The modeling and optimization technique presented in this paper will provide airport and airspace designers with a host of alterative trajectory options for analysis of potential landing sites, associated traffic procedures, and entry options, as shown by the presented BWI case study.

Nomenclature

C_T	=	thrust coefficient
D	=	rotor drag, lb
g	=	gravitational constant, ft/s^2
R	=	rotor-blade radius, ft
SFC	=	specific fuel consumption, lb/(hp $*$ hr)
t	=	time, s
V	=	flight velocity, kn
$\dot{V}$	=	acceleration, ft/s^2
W	=	helicopter weight, lb
x	=	ground coordinate with direction from west to east, ft
y	=	ground coordinate with direction from south to north, ft
z	=	coordinate upward, ft
α_{TPP}	=	main rotor tip-path-plane angle, deg
β	=	flight-path lateral angle (in xy plane), deg
γ	=	flight-path longitudinal angle (in xz plane), deg
θ	=	noise radiation sphere elevation angle, deg
μ	=	advance ratio, $V/\Omega R$
ψ	=	noise radiation sphere azimuth angle, deg
Ω	=	rotor angular rotation, 1/s

I. Introduction

THE increasing demand for commercial air transportation results in delays given airspace bottlenecks resulting from queues along final approach and departure corridors. In urban areas, it is often infeasible to build new runways, and regardless of automation upgrades traffic must remain separated to avoid the wake of previous aircraft.

Runway-independent aircraft (RIA) have been proposed to increase passenger throughput by offloading short- to medium-haul (<400 n miles) traffic from overcrowded runways, utilizing stub runways or vertiports as alternative landing sites. RIA candidate designs include high-capacity vertical takeoff and landing (VTOL) vehicles as well as powered-lift fixed-wing extremely short takeoff and landing (ESTOL) vehicles. Introduction of RIA traffic patterns in crowded terminal airspace has the potential to increase air traffic controller workload, creating new conflict-related delays rather than alleviating congestion. Simultaneous noninterfering (SNI) approach and departure procedures for RIA will minimize air traffic control overhead and maximize overall throughput.[1] SNI paths do not intersect existing traffic corridors, and so RIA SNI arrivals and departures can be sequenced independent of fixed-wing traffic. By definition, SNI trajectories occupy previously unused airspace and thus can overfly noise-sensitive communities previously undisturbed by fixed-wing traffic. As new SNI routes are proposed, public acceptance mandates the development of noise abatement procedures (NAP). RIA approach and departure routes must also be acceptable to pilots and air traffic controllers (ATC), comfortable for passengers, and economical for the airlines.

In previous work,[2] we developed a methodology for optimizing longitudinal plane two-dimensional RIA trajectories, with results illustrating the properties of the optimization tool and low-noise SNI solutions for a rotorcraft as the RIA. This work extends the trajectory optimization model to three dimensions, incorporates population data into the objective function, and focuses on a practical case study: the design of SNI RIA approach procedures to Baltimore–Washington International (BWI), a rapidly growing urban airport.

The goals of this research are to provide a segmented route optimization tool that enables identification of acceptable three-dimensional RIA NAPs and to study the design of noise-optimal SNI procedures for a rotorcraft on approach to BWI. Our tool rapidly enables airport planners, controllers, and pilots to define trajectories with respect to cost (radiated ground noise for this work), providing solutions to be subsequently ranked in terms of pilot and ATC workload, impact on fixed-wing traffic, and safety.

Noise abatement for fixed-wing aircraft has received significant attention. Studies have determined that pilots prefer to fly the simplest single-segment trajectories available,[3] resulting in the adoption of continuous descent approaches[4] that simultaneously lower noise and fuel use as a result of reduced engine thrust. Researchers have also proposed the optimization of approach[5] and departure[6] trajectories over fuel and noise cast as number of awakenings, computed from a model of radiated ground noise and population density. In such work, numerical optimization techniques identify a continuous (or piecewise continuous) optimal trajectory, enabling accurate

Presented as Paper 2005-0909 at the AIAA 43rd Aerospace Sciences Meeting and Exhibit, Reno, NV, 10–13 January 2005; received 21 January 2005; revision received 11 April 2005; accepted for publication 24 April 2005.

*Graduate Research Assistant, Aerospace Engineering Department; minxue@glue.umd.edu. Student Member AIAA.

†Assistant Professor, Aerospace Engineering Department; atkins@glue.umd.edu. Senior Member AIAA.

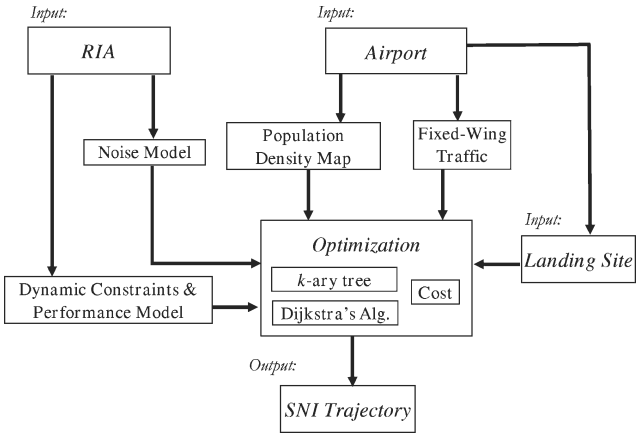

Fig. 1 Optimization of segmented SNI trajectories.

computation of objective function quantities such as noise, fuel, and time. As an alternative approach, segmented routes[7] have been designed to facilitate comprehension by pilots and ATC and to enable specification as procedures available for cockpits with and without advanced automation.

Our work is distinct from previous NAP development in its construction of strictly SNI routes described by a sequence of trimmed flight segments that connect initial approach and landing sites. Figure 1 shows the models and algorithms we integrate to build optimal segmented SNI trajectories. Performance and noise models must be provided for each RIA to be operated. In some cases (e.g., rotorcraft vs fixed-wing ESTOL), model differences can result in optimized SNI trajectories with significantly different characteristics, a problem that must be addressed at the systems level should a mixed RIA fleet emerge. For each airport, the surrounding population and airspace use must be characterized, and a RIA landing site must be identified. Once models are complete, the terminal-area airspace is decomposed as a k-ary tree, and Dijkstra's search algorithm is employed to find an optimal solution over the discrete search space.

This paper begins with a description of our discrete optimization method and the objective function used to generate SNI NAPs. Next, we present the performance and noise model[8] for an AH-1 rotorcraft, the RIA studied in this work. For BWI airport, a RIA landing site is identified, and population data are compiled from 2000 census data. To find strictly SNI routes, typical BWI East-flow traffic operations are surrounded by safe separation zones and modeled as impenetrable obstacles. Candidate AH-1 NAPs are presented to illustrative how population density, aircraft flight envelope limitations, and entry region influence final trajectory shape and corresponding velocity profiles.

II. Trajectory Optimization Algorithm

Individual aircraft trajectories can be mathematically optimized and precisely followed by existing autopilots with advanced navigation and control technologies. However, segmented routes[7] enable intuitive comprehension by pilots and ATC, facilitate communication of trajectory, and typically reduce computational complexity relative to complex numerical global optimization processes. For this work, SNI final approach trajectory optimization is defined as a two-point boundary-value problem in three dimensions, and "optimized" noise abatement procedures are described by a sequence of one or more segments, each with constant velocity or acceleration. As described by Latombe,[9] several techniques, including roadmap, potential field, and cell decomposition, exist for motion planning in obstacle fields. Probabilistic roadmap[10] and the rapidly exploring random tree[11] are currently popular motion/path planning techniques. Most of these methods were developed for ground robots with few motion constraints or for identifying nonoptimal solutions quickly, whereas, in our case, the complex cost [blade-vortex interaction (BVI) noise database + population distribution] must be optimized in the presence of dynamic constraints and impenetrable airspace obstacles. Given these requirements, an incremental search method, which couples k-ary tree decomposition and Dijkstra's algorithm, is adopted for this work.

A. Decomposition Strategy

In previous work,[2] we utilized a cell decomposition strategy that could model arbitrary obstacles, guarantee globally optimal results limited only by discrete cell size, and allow arbitrarily complex cost functions f. In three dimensions, however, it is difficult to manage computational complexity when sufficient resolution is present in the discretized cell map. To better manage complexity, we now represent the search space as a k-ary tree, defined as a search space with no more than k children for each node. As a preliminary to k-ary tree construction, we impose dynamic parameter constraints well within limits of both the performance envelope and passenger comfort. For longitudinal flight, limits are placed on flight-path angle γ and acceleration $\dot{V}$, with the addition of parameter β for three dimensions to represent the change in heading between flight segments. The goal with our algorithm and this simple parameter space is to facilitate global optimization over experimentally verified noise and performance models. In current work, we assume the transition between flight segments is instantaneous and incurs no additional cost, an imprecise but necessary assumption given that work is still underway to develop a noise model for our RIA (the AH-1 helicopter) that is valid during trim state transitions and not computationally expensive to derive for each optimization iteration.

Given these dynamic parameter restrictions, we use four control variables γ, $\dot{V}$, β and Δd, where Δd is the distance step in the lateral (xy) plane and along the direction of radius of the circle whose origin is located at the touchdown site. Note that the set of control variables is reduced to three variables γ, $\dot{V}$, and Δx when restricting solutions to two dimensions (longitudinal plane) only. For two- and three-dimensional cases, control variables are discretized, and the combinations over these variables form an upper bound of the branching factor for our k-ary tree.

An incremental method in which the search tree is expanded until the final solution is found is adopted for our work. At each iteration, the next available k-ary tree node is selected by the search algorithm in order of increasing cost, as discussed next. When exploring a k-ary tree node, k candidate "child" nodes are generated. To minimize search-space size, new nodes are merged with existing nodes if they are in a small "error box," which denotes approximately the same velocity and spatial position in which geometric (x, y, z) coordinates match to within a specified tolerance. This decomposition and merging strategy is shown in Fig. 2 for the spatial view without control variable V. For two-dimensional optimization (e.g., approach in the longitudinal plane), our previous cell decomposition[2] and new k-ary tree strategies are comparable in representational ability and efficiency. For three-dimensional trajectories, the k-ary tree enables more accurate representation, and node merging efficiency improves significantly. The pseudocode for the k-ary tree decomposition strategy is shown next in procedure *TreeBuild* (Fig. 3), where M, N and R are the resolutions of γ, β, and V, respectively. For this work, these intervals are set as $\Delta\gamma = 1$ deg, $\Delta\beta = 4$ deg, and $\Delta V = 3$ kn. During expansion of a node *enode*, the procedure identifies all child nodes and inserts them into the node stack if they are not merged and if the connecting path from *enode* does not *Intercept* any fixed-wing airspace obstacles. These nodes are marked as the neighbors of *enode*, and their tree level (segment number) is incremented relative to *enode*.

B. Search Algorithm

Given landing site boundary condition $[x_f, y_f, (z_f), V_f]$, approach boundary constraints $[x_{\text{init}}, y_{\text{init}}, (z_{\text{init}}), V_{\text{init}}]$, and our segmented solution requirement, Dijkstra's optimal search algorithm with average computational requirements significantly lower than those of dynamic programming[12,13] was employed to minimize the number of expanded search states. (z_f and z_{init} are not included in two-dimensional case.) Dijkstra's algorithm explores nodes in order of increasing value of cost function $g(n)$, the accumulated cost from the initial state to search node n. For this *Search* algorithm shown

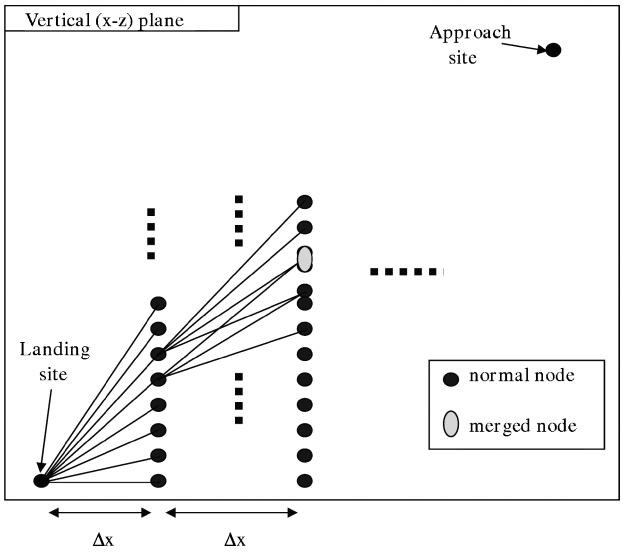

a) Side view

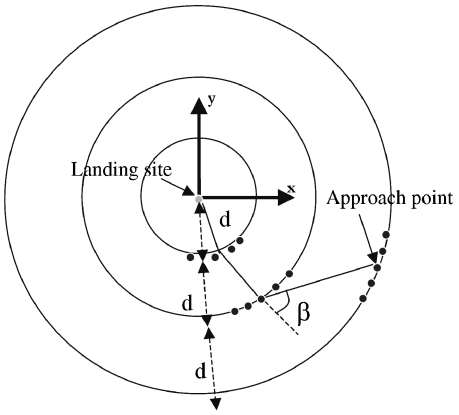

b) Top view

Fig. 2 The *k*-ary tree decomposition and merging (spatial view).

```
Procedure TREEBUILD(enode, nodes, obstacles)

global γ[M], β[N], V[R], Δd;
Node nnode;
begin
  for each combination of γ[i], β[j], V[k], Δd do
    (x, y, z, V[k]) ← CalculateState(γ[i], β[j], V[k], Δd, enode);
    nnode ← new Node (x, y, z, V[k]);
    nnode.level ← enode.level + 1;
    if not Merge(nnode, nodes) and not Intercept(nnode, obstacles) do
      push nnode into stack enode.neighbor;
      nnode.cost ← ∞; nnode.status ←′ open′;
      push nnode into stack nodes;
    end
  end
end
```

Fig. 3 *TreeBuild* algorithm.

in Fig. 4, the inputs are the nodes stack built so far, number of flight segments, landing state, and initial approach state. Here c is the cost from explored node u to a neighboring successor node. Because we are searching backward, the landing state/node is initially placed on the *nodes* stack. Then, the main loop expands the node with minimum cost, creating its child nodes and ordering them in the updated stack by cost. The loop terminates when the minimum-cost node is within the desired approach state region.

This Dijkstra algorithm with k-ary search-space decomposition is a global optimization technique. However, the solution is optimal

```
Procedure SEARCH(nodes, segnum, land, appr)

integer segnum;
Node land, appr, u;
begin
  push land into stack nodes;
  u ← land; land.level ← 0; land.cost ← 0; appr.cost ← ∞;
  while (u ≠ appr) do
    u ← FindMin(nodes);
    if (u = NULL) break ;
    else
      u.status ←′ closed′;
      if (u.level < segnum − 1) then TreeBuild(u, nodes);
      else push appr into stack u.neighbor;
      for each adjacent node n_i of u do
        if (n_i.status ≠′ closed′) then c ← FindCost(n_i, u);
          if (u.cost + c < n_i.cost) then
            n_i.cost ← u.cost + c; n_i.previousnode ← u;
  end
end
```

Fig. 4 *Search* algorithm.

```
Procedure ITERATIVEDEEPENING(land, appr)

integer i, j, k;
float cost, segnum, newcost;
Node land, appr;
Node stack solution, nodes;
begin
  cost ← 0; segnum ← 2; solution ← NULL;
  do
    Search(nodes, segnum, land, appr);
    solution ← Path(appr);
    newcost ← solution.cost; D ← |newcost − cost|;
    cost ← newcost; segnum ← segnum + 1;
  while D ≥ εandt < tmax
  return solution;
end
```

Fig. 5 *IterativeDeepening* algorithm.

only with respect to the level of discretization when dividing the continuous space into a segmented path. Theoretically, this error can approach zero with infinite resolution on the search variables γ, $\dot{V}$, and β; however, computational complexity and path complexity also increase with resolution.

We have wrapped an iterative deepening strategy[14] around the search algorithm to identify optimal trajectories with two to n segments, enabling insight into the effect of discretization on solution properties. Initial low-resolution solutions are simple (few segments) but can be costly. Higher-resolution solutions approach the globally optimal cost but will contain numerous flight segments that would only be feasible as standard flight procedures given a capable autopilot that could follow arbitrary continuous flight trajectories. Our iterative deepening procedure is shown in Fig. 5. In our work, we halt at a resolution where the difference between current and last cost is within a user-defined threshold ε or a maximum execution time is exceeded. In practice, this solution serves as an anytime algorithm,[15] allowing both the software monitor and the pilot/airport planner to break the planning loop to obtain intermediate solutions with lower resolution (e.g., small number of flight segments).

C. Cost Function

Trajectory optimization tools require an objective function $g(n)$ to measure proposed solution quality. Typically, $g(n)$ includes time and fuel penalty terms, weighted by pilots/airlines based on their relative priority. NAP design also requires a term to represent radiated ground noise. For SNI airspace design, the cost function J_n for trajectory optimization over an n-segment trajectory is given by

$$J_n = \sum_{i=1}^{n} \left[c_1 \times N_{i,i-1} \times t_{i,i-1} + c_2 \times t_{i,i-1} + c_3 \times m_{(\text{fuel})i,i-1} \right] \quad (1)$$

In this expression, $t_{i,i-1}$ is the duration for the single trajectory segment between boundary nodes i and $i-1$, and $m_{(\text{fuel})i,i-1}$ is the total fuel consumed in this time period. Noise energy is given by $N_{i,i-1}$ for each segment, and $c_{1,2,3}$ are adjustable weights for noise, time, and fuel, respectively. A weight sensitivity study for two dimensions has been performed in previous work.[2] In this three-dimensional work, our goal is to develop the best noise abatement procedures, thus, c_2 and c_3 are set to zero while $c_1 = 1$.

III. Case Study: AH-1 Approach to BWI

The preceding optimization algorithm and cost function are applicable to any RIA design and any airport. To investigate its practical use, we provided our SNI RIA NAP optimization procedure with performance and noise models for an AH-1 rotorcraft and traffic and population models for BWI airport, as shown in Fig. 6. These models are described in detail next.

A. AH-1 Performance and Noise Models

Our optimization procedure requires constraints on three optimization parameters: γ and $\dot{V}$ for the longitudinal plane and β for the lateral plane. A fairly typical set of limits for the AH-1 that do not approach performance or passenger comfort limits were imposed. Flight-path angle γ is limited to $(-9 \text{ deg} \le \gamma \le 9 \text{ deg})$, while acceleration $\dot{V}$ is limited to $(-0.05g \le \dot{V} \le 0.05g)$. The γ constraint is based on performance and safety limitations, whereas $\dot{V}$ is limited more from passenger comfort than performance considerations. The maximum heading change β between segments is set to $(-80 \text{ deg} \le \beta \le 80 \text{ deg})$, a fairly generous limit representing a tradeoff between exploring a large solution space vs supporting our assumption that trim state transitions are instantaneous and without cost.

As just described, the full optimization objective function includes time, fuel, and noise terms to enable efficient and quiet procedure designs. Time is directly computed from flight trajectory path length and velocity; fuel use up to a time t_i is derived from a standard rotorcraft model[16]:

$$m_{\text{fuel},i} = \sum_{k=1}^{i} SFC \times HP_k \times t_k \tag{2}$$

where HP_k is power required per hour for trim flight segment k, and t_k is the corresponding time. HP_k can be expressed as

$$HP_k = \rho A(\Omega R)^3 \left[\frac{kC_T^2}{2\mu} - \mu\alpha_{\text{TPP}} C_T + \frac{sC_{d0}}{8(1+4.6\mu^2)} \right] \tag{3}$$

where $\alpha_{\text{TPP}} = -D/W - \gamma - \dot{V}/g$, D is a function of $[V - f(V^2)]$, and $\mu = V/(\Omega R)$. $\rho A(\Omega R)^3$, C_T, s, C_d0, and k can all be treated as rotorcraft model-specific constants during approach. Although engine power should include tail rotor power and installation losses, these are secondary effects not necessary for this work until we incorporate the effects of transitions between flight segments. Given these expressions, fuel consumption is a function of V and γ.

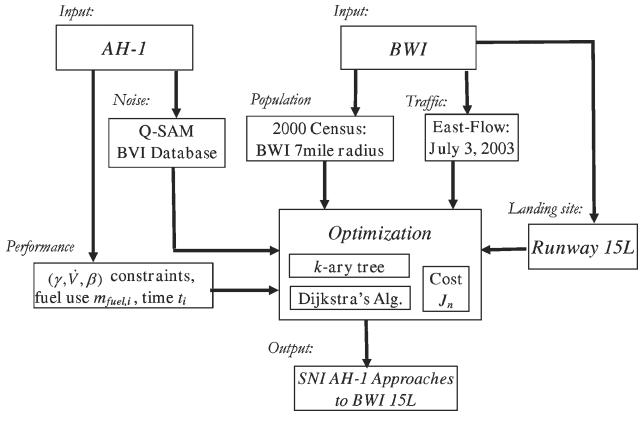

Fig. 6 Models for SNI AH-1 approach design to BWI runway 15L.

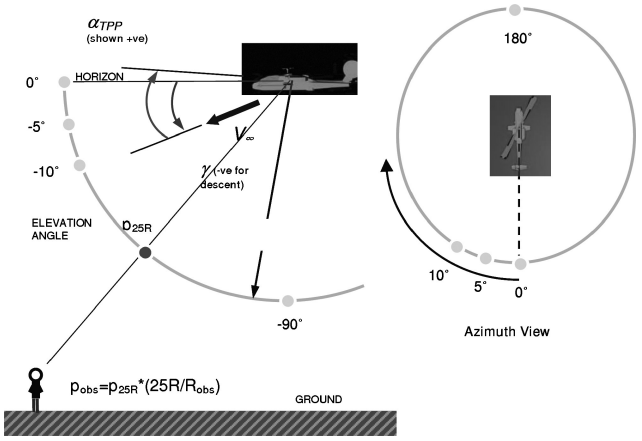

Fig. 7 Q-SAM BVI noise model.

For any rotorcraft or tiltrotor after conversion to helicopter mode, the dominant noise source on approach is BVI.[8] Other noise sources (e.g., engine) are of increasing importance during departure, where maximum power is required and vortices are well below the rotor blades. BVI noise is the typical popping or slapping sound that radiates significant acoustic energy far from its source. For the AH-1, BVI noise is computed with the experimentally verified quasi-static acoustic mapping (Q-SAM) method devised by Gopalan et al.[8] and conceptually depicted in Fig. 7. The output is the A-weighted sound exposure level (SEL) expressed in decibels. Here R_{obs} is the distance between the observer and the vehicle, elevation angle θ is counterclockwise and starts from the horizon, and azimuth angle ψ is clockwise with zero angle pointing back from the rotorcraft. Spherical distributions of radiated noise are developed as a function of tip-path plane angle α_{TPP} and advance ratio μ. Interpolation is performed when the observer is not located at the exact grid point of the sphere defined in the noise database. In the quasi-static model, rotorcraft trim state transitions (e.g., longitudinal path angle, lateral path angle) are presumed instantaneous, and we do not include effects from atmospheric absorption, wind, temperature, or ground reflection. Given a segment (two extreme ends i and $i-1$) with constant γ and $\dot{V}$, for an observer on the ground the BVI noise would be

$$P_{i,i-1} = q\left(\alpha_{\text{TPP}_{i,i-1}}, \mu_{i,i-1}, R_{\text{obs}_{i,i-1}}, \theta_{i,i-1}, \psi_{i,i-1}\right) \tag{4}$$

where P refers to the average A-weighted sound exposure level SEL_{av} expressed in decibels and $R_{\text{obs}_{i,i-1}}$ is the average observer distance. To provide intuition, Fig. 8 shows approximate trends of BVI noise for different flight speeds.[2]

B. BWI Terminal-Area Population and Traffic Models

Because segmented trajectories must be designed to minimize noise over populous areas, we employ a cost function in which noise propagated to the ground is weighted by population density. BWI area population data was downloaded from the year 2000 census.[‡] Figure 9a shows the population distribution around BWI. The blocks with darker red denote high population density areas, while lighter red represents low density. For this work, only the blocks within seven miles of BWI airport are taken into account, as illustrated in Fig. 9a. We define noise "cost" as the sum of the noise experienced over a set of ground-based microphones, where the noise at each microphone is weighted by the population density of the region surrounding that microphone. Evenly spaced microphone locations (Fig. 9b) capture most information, but such a design can also neglect the small dense-population blocks shown in Fig. 9a. To prevent this, a large number of microphones must be modeled, and computational

[‡]Data available online at http://www.esri.com/data/download/census2000_tigerline/index.html/ [cited Aug. 2004].

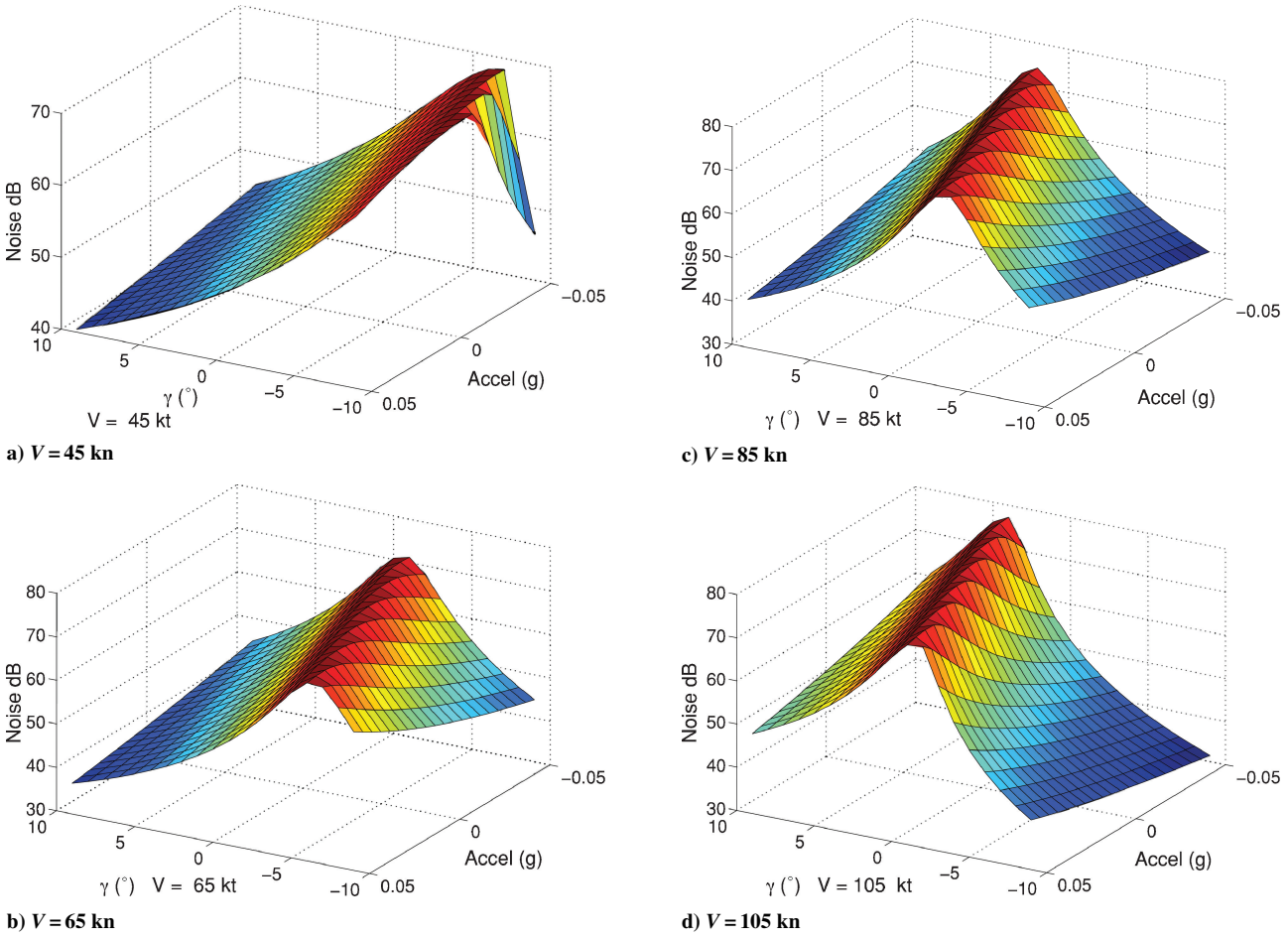

Fig. 8 AH-1 BVI noise characteristics.

cost will be prohibitive. In this work, to get an accurate representation of noise in reasonable computational time we define the center points of the Fig. 9a population blocks as "microphone locations" for a ground noise measurement matrix over which noise is normalized (see Fig. 9c). Because, intuitively, the noise annoyance should be worse when the air vehicle flies over the dense-population areas, we set the importance of each block based the density instead of the total population. Thus, cost function penalty weight for each microphone is proportional to the population density at that site. Figure 9 also shows the position and orientation of the inertial reference coordinate system, in which the z coordinates coincide with altitude.

Combining Q-SAM noise data with population density, total noise energy over all K microphones for a single trajectory segment is computed as

$$N_{i,i-1} = \frac{\sum_{k=1}^{K} 10^{P_{i,i-1}/10} \times W_k}{\sum_{k=1}^{K} W_k} \tag{5}$$

where each W_k is the population-based weighting factor for microphone k. Total cost over all n trajectory segments is

$$J_n = \sum_{i=1}^{n} N_{i,i-1} \times t_{i,i-1} \tag{6}$$

where $t_{i,i-1}$ is the duration for this single trajectory segment between boundary nodes i and $i-1$. The optimization goal given our iterative deepening strategy is then to progressively find solutions for $n = 1, 2, \ldots, n_{\max}$ defined as trim flight segment sequences that minimize cost J_n.

C. BWI Fixed-Wing Traffic Obstacle Model

To explore strictly SNI noise-optimal trajectories, flight track data were acquired for BWI airport. Daily approach and departure tracks for the BWI terminal area can typically be grouped into either east flow or west flow, depending on prevailing wind direction. In our work, track data for all arrivals and departures on 3 July 2003 were utilized as a sample for east-flow operations.

Figure 10 shows track data top and side views and also presents the BWI runway layout. Because of their shorter length, runways 33R/15L are statistically much less used, representing 3–4% of all 2003 operations.[17] Given also that when used 33R/15L primarily support smaller general aviation/business jet traffic, operations utilizing this short runway can be removed from consideration without significant impact on passenger throughput.

We adopt 33R/15L as the BWI runway for our new RIA traffic, a choice that will support both VTOL and ESTOL RIA operations without expansion to the BWI runway system. (Although important before practically implemented, the effect of the 33R/15L RIA landing site choice on ground operations is beyond the scope of this research.) With few outliers, we wrapped the existing east-flow fixed-wing flight tracks in a set of cylinders and cones to define no-fly areas for SNI operations. For our case study, traffic obstacles are modeled below 4000 ft, a ceiling also placed on RIA approach trajectories. As a comparison with flight track data, top and side views of our obstacle field are shown in Fig. 11. The set of obstacles is enlarged to enforce a 1000-ft clearance constraint and treated as impenetrable. To support the east-flow traffic model, the new RIA is constrained to land near the approach end of runway 15L, parallel to fixed-wing traffic departing from 15R.

IV. Simulation Results

Based on the AH-1 and BWI models just presented, we now study the design of noise-optimal SNI approach trajectories for BWI airport. For all approach cases, the initial velocity is prescribed as 95 kn and final velocity 45 kn, typical values for an AH-1. The trajectory spans the area within seven miles (approximately 40,000 ft) from

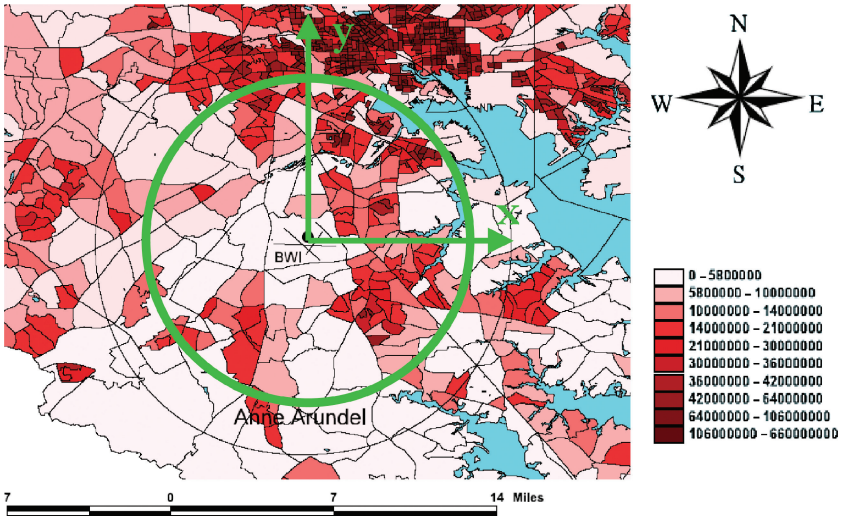

a) Population distribution

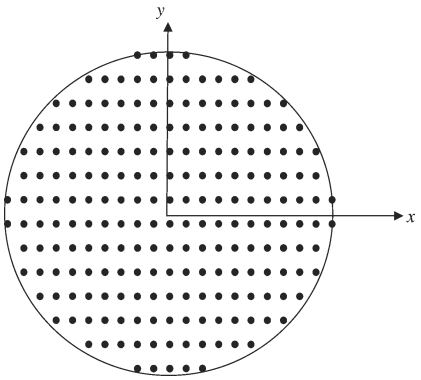

b) Evenly spaced matrix

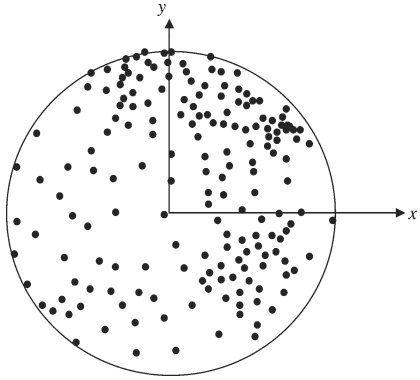

c) Matrix based on population blocks

Fig. 9 Population distribution map (BWI) and measurement matrix.

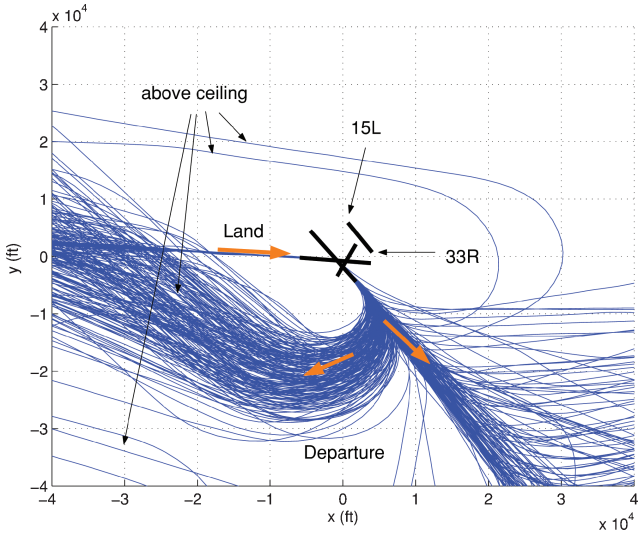

a) Top view

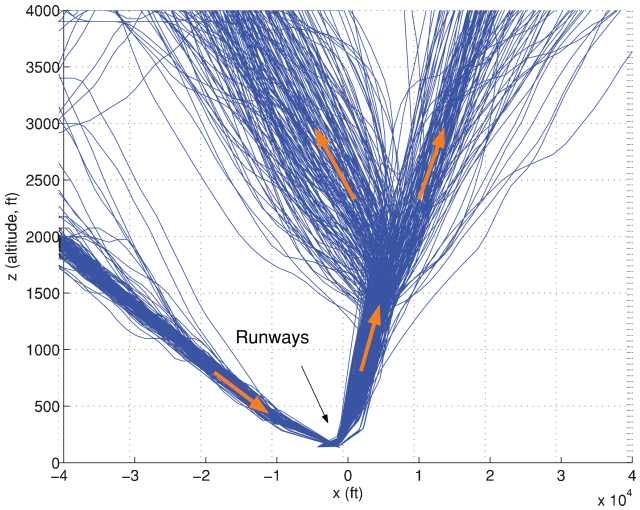

b) Side view

Fig. 10 East-flow operation at BWI airport: 3 July 2003.

BWI and to a ceiling of 4000 ft, whereas the lowest altitude is 100 ft, given that the Q-SAM noise model is only valid above 100 ft and that population is not dense near the touchdown site. For distinction, dB-PD is defined as the unit of 10 log J_n, which represents the population-density weighted noise cost over the area just defined.

A. Two-Dimensional Results with No Obstacles

As a connection to our previous work,[2] we built a set of two-dimensional trajectories, in which the helicopter approaches from state ($x = 40{,}000$ ft, $y = 0$ ft, $z = 2000$ ft, $V = 95$ kn) to state ($x = 0$ ft, $y = 0$ ft, $z = 100$ ft, $V = 45$ kn) with no lateral turning permitted and no landing orientation specified. Note that coordinates are defined such that z represents altitude above the runway (~above ground level) and x toward east. As shown in the Fig. 12 approach with flight track from right to left on the page, a noise-optimal longitudinal-plane approach is a sequence of accelerating climbs and decelerating descents, a "bang-bang" solution that always utilizes saturated tip-path-plane angle α_{TPP}. From the BVI

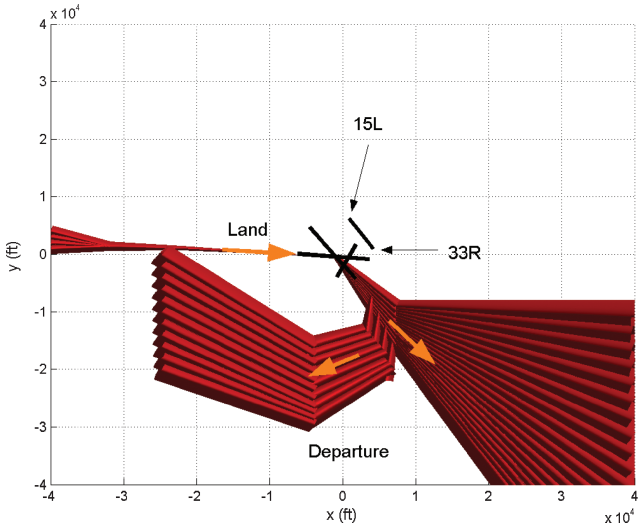

a) Top view

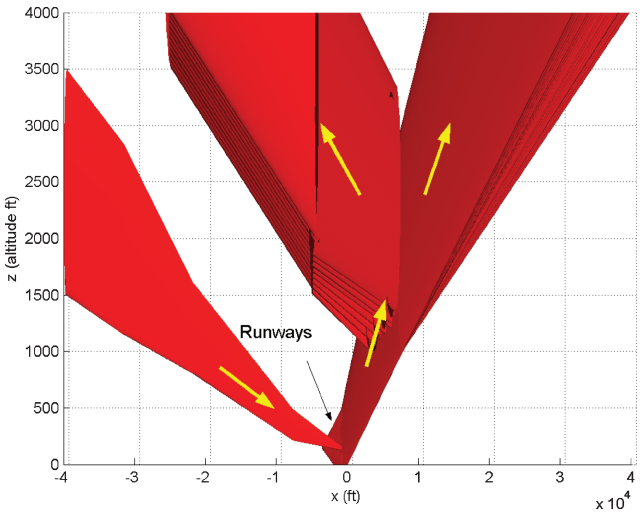

b) Side view

Fig. 11 Obstacles modeled for east-flow operation.

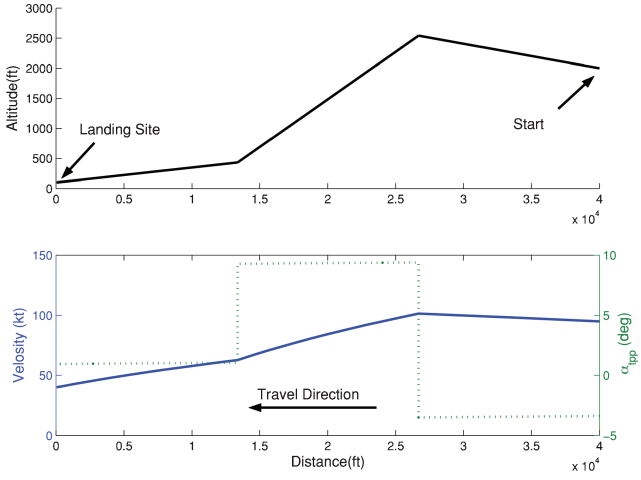

a) Path, velocity, and α_{TPP} profile (longitudinal plane)

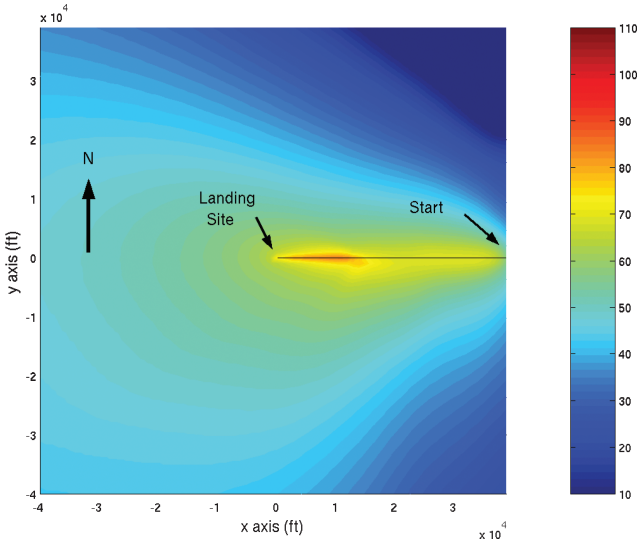

b) BVI SEL distribution (top view)

Fig. 12 Two-dimension three-segment noise-optimal trajectory.

noise perspective, this result maximizes the distance of the wake from the rotor, thereby minimizing vortex-induced noise.

Application of our iterative deepening algorithm enables comparison between different numbers of approach segments, the results of which are provided in Fig. 13 for a longitudinal-plane approach. Figure 13 shows the longitudinal-plane path and velocity, the BVI SEL distribution, execution time, and noise index cost from Eq. (6). All cases are run on a 2.8-GHZ Linux platform. As shown in the figure, although the path becomes increasingly complex, the optimizer is better able to design a path that reduces BVI noise, illustrating the tradeoff between path complexity and noise.

B. Three-Dimensional Results with No Obstacles

For this case, the three-dimensional approach problem is defined from start state ($x = -28{,}000$ ft, $y = -28{,}000$ ft, $z = 2000$ ft, $V = 95$ kn) to final state ($x = 1000$ ft, $y = 5000$ ft, $z = 100$ ft, $V = 45$ kn) approaching the runway 15L threshold, which means the rotorcraft flies from the southwest approach corner to the landing site. Optimal solution behavior is similar to two-dimensional cases. Figure 14 shows the three-segment solution path and velocity profiles and the ground noise distribution (SEL). Figure 15 illustrates the tradeoff between path complexity (represented as number of flight segments) and noise cost. Note, however, the rapid increase in optimization execution time as number of segments increases caused by the increase in search-space size as the k-ary tree is built to a greater three-dimensional depth. Although there is a computational bound on the total number of three-dimensional flight segments that can be explored, we do not view this as a significant limitation because neither pilot nor air traffic controller will want to manage an approach procedure with more than three to five distinct low-altitude segments. Our goal is to build SNI procedures that can be studied and adopted as standard for each RIA landing site, favoring identification of globally optimal results over real-time computation.

C. Effects of Population Density Weighting

Previous results were optimized over the cost function from Eq. (6) that included population-based weighting factors. To investigate the effects of population density weighting, we set all population weights W_k to 1.0 (uniform density distribution) and recomputed a representative three-segment three-dimensional approach. Consider an approach with start state ($x = -40{,}000$ ft, $y = 10{,}000$ ft,

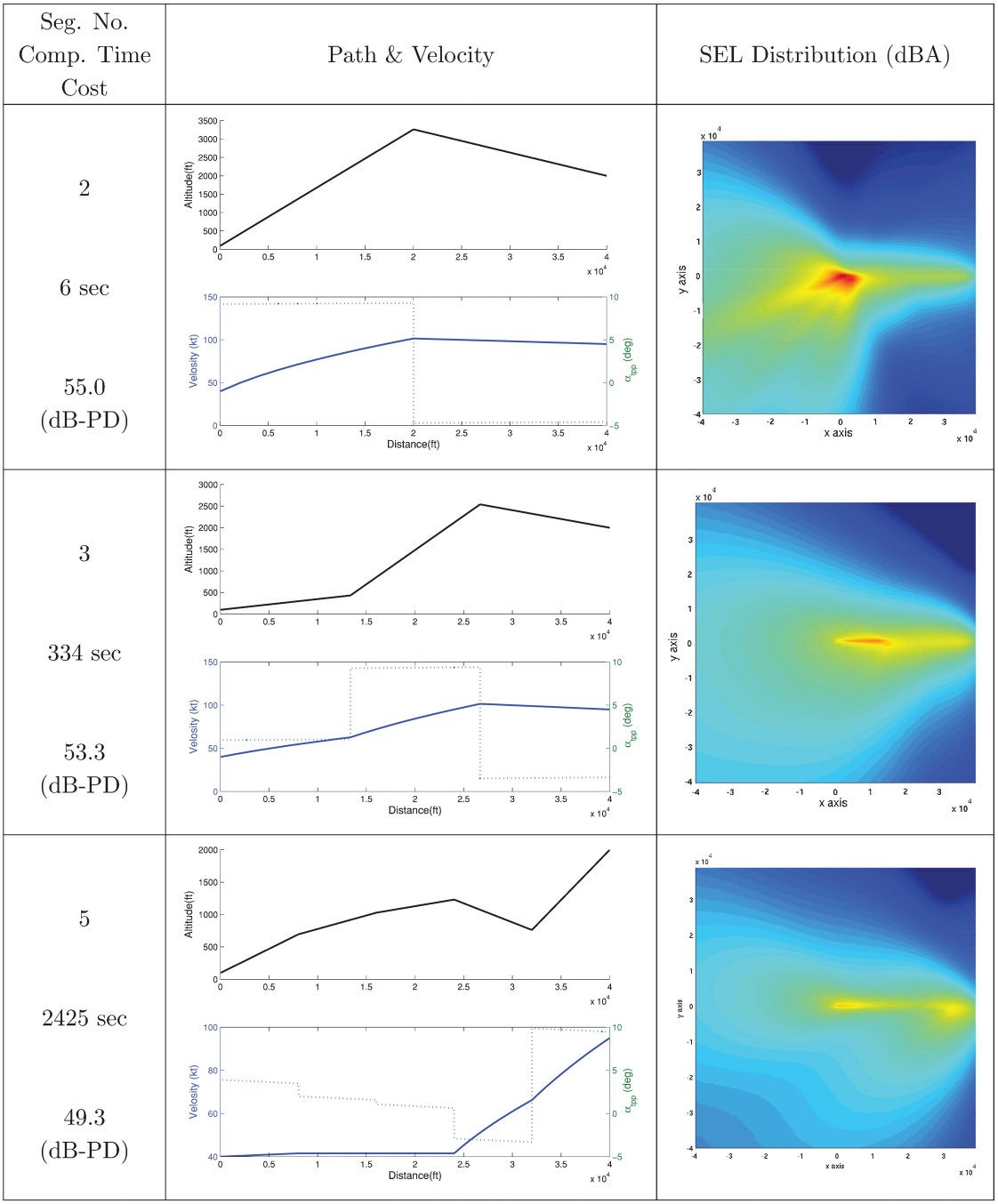

Fig. 13 Comparison with varying segment number in two dimensions.

$z = 2000$ ft, $V = 95$ kn) to final state ($x = 1000$ ft, $y = 5000$ ft, $z = 100$ ft, $V = 45$ kn) landing on runway 15L. A comparison of population-weighted and uniform cost weight trajectories is provided in Fig. 16. Figures 16a and 16b show the case with no effect of population density distribution, while Figs. 16c and 16d present the case with population weighting. It is shown that, although the total noise integrated over the entire trajectory is lower for uniform density weighting, inclusion of the population weighting terms yields a result with significantly lower noise over the region around point A and C, the high-population areas.

D. SNI Noise-Optimal Trajectories

The practical objective of this work is to design SNI approach procedures for RIA. To illustrate the use of our design tool and to show that SNI approaches are feasible at a major airport (BWI) without altering existing fixed-wing procedures, we conducted a series of optimization runs with traffic obstacles as well as the population and BVI noise models just used.

As described earlier, east-flow traffic at BWI on 3 July 2003 is modeled as a set of impenetrable cylinders and cones for our RIA approach design optimization tool. Rather than finding a single optimal solution, we identified optimal solutions for each approach entry quadrant, facilitating direct approach interception rather than an extended entry that circles far around the BWI terminal area. The entry regions in which the optimizer can place its initial approach fix represent heading quadrants (NE,NW,SW,SE) of $>$ seven-mile radius with altitude above 2000 ft (shown in Fig. 17b). AH-1 approach trajectories were optimized for each region.

Figure 17a gives the four locally optimal trajectories for runway 15L, while Figs. 17c–17f show the SEL distribution. The final solutions for sectors I and II are similar, utilizing constant descent followed by decelerating climb and descent, a reasonable low-noise solution given the velocity-dependent BVI noise profiles as shown

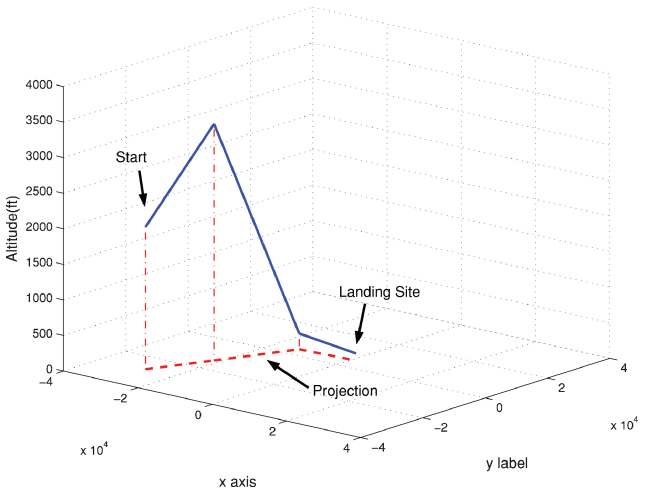

a) Path shape

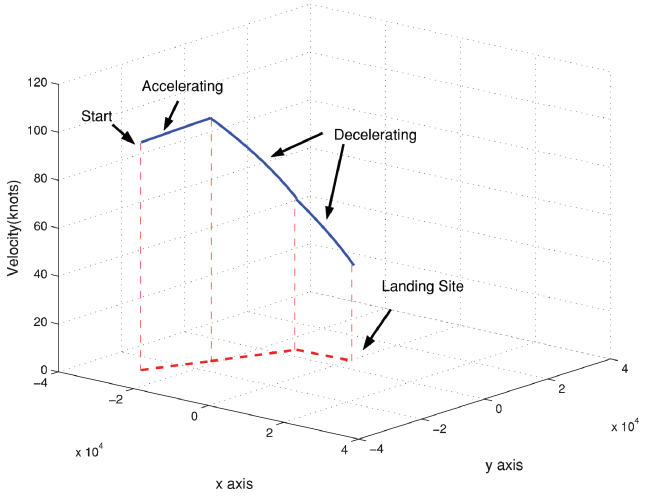

b) Velocity profile

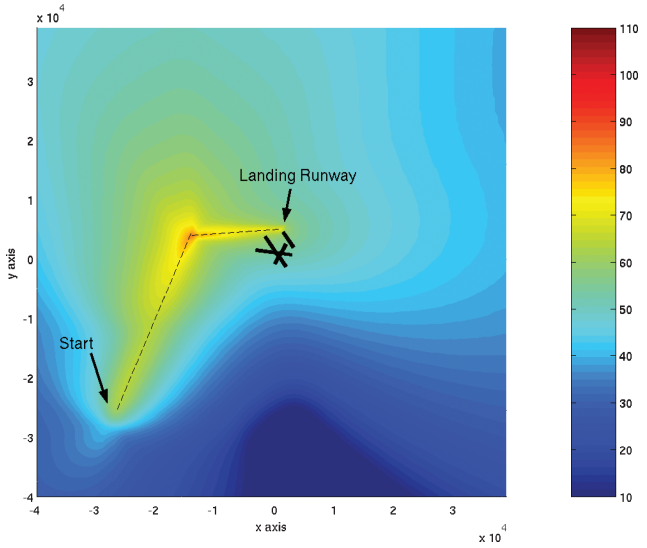

c) BVI SEL distribution (top view)

Fig. 14 Three-dimension three-segment noise-optimal trajectory.

Table 1 Comparison of SNI noise-optimal trajectories

Sector	Cost (10 log J_n), dB-PD	People exposed to noise > 60 dBA	Fuel consumption, lb	Flight time, s
I	48.4	981	28.1	444
II	45.6	0	26.1	417
III	53.0	9,301	26.0	440
IV	55.0	19,991	28.4	481

in Fig. 8. The optimum sector III trajectory climbs over the aircraft on final approach, then descends to approximately join the final segment from the sector I/II solutions. For sector IV, the optimal SNI solution must avoid the traffic departing from runway 15R, similarly following an alternating climb/descent path to landing. Table 1 shows the numerical comparison between these four solutions. (The "0" number of people exposed to noise greater than 60 dBA might not be precise because our microphone matrix might not capture the highest noise area if it is too sparse.) First, perhaps the most significant conclusion is that for real RIA and airport models, not only can one SNI approach be found, but in fact SNI approaches of varying quality can be identified for all entry sectors. The sector II solution is best from a noise perspective and would be the best default procedure identified in this study. The sectors III and IV solutions enable more efficient approaches for traffic entering from the south and also are acceptable from a noise perspective, particularly if used infrequently.

Given the proximity of the sectors I and II solutions, we propose routing traffic in three sectors (red dashed lines in Fig. 17b), favoring the lowest-noise approach from the north. By this means, all RIA traffic entering from the southwest and southeast would fly the trajectory from Figs. 17e and 17f, respectively, whereas all traffic from the north would utilize the trajectory from Fig. 17d.

In practice, airport planners judge noise with an integrated day-night average sound level descriptor (DNL),[17] which is a composite noise index derived from a 24-h average noise level with a weighting factor of 10 dB applied to noise events occurring during nighttime periods. Thus, our SEL distribution could be converted to DNL through

$$\mathrm{DNL} = 10 \times \log\left(10^{SEL_{\mathrm{pf}}/10} \times \frac{\text{flightsperday}}{\text{duration}}\right) \tag{7}$$

where the SEL_{pf} is SEL per flight. Because only daytime operations are considered, the duration is to be 15 h. (The period from 2200 to 0700 hours is defined as "night.") The DNL distributions for the sector II AH-1 solution are shown in Fig. 18. Totals of 100 and 300 flights per day represent 6.6 flights/h and 20 flights/h, respectively. As a reference,[17] 65 DNL or less is considered an acceptable level for residences, schools, hospitals, whereas 70 DNL or less is acceptable for hotels, playgrounds, etc. The BVI-related DNL distributions for the AH-1 on approach to BWI are low compared with the normal operations[17] in BWI, where some areas are even affected by 75 DNL.

Seg. No. Comp. Time Cost	Path	Velocity	SEL Distribution (dBA)
2 42 sec 57.7 (dB-PD)	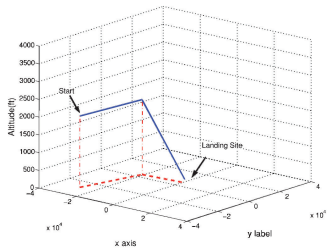	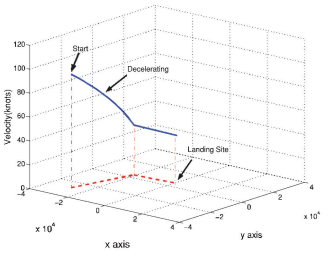	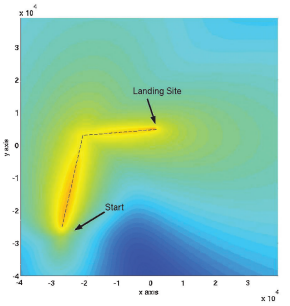
3 44975 sec 48.2 (dB-PD)	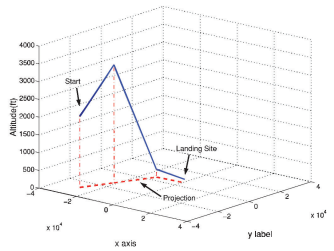	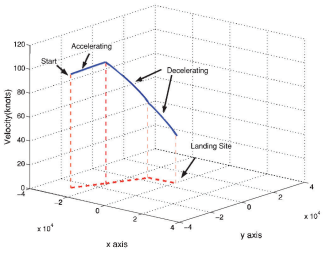	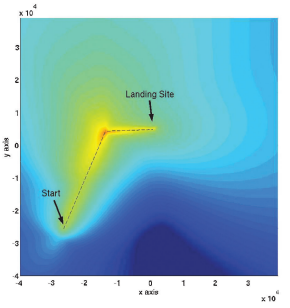

Fig. 15 Comparison with varying segment number in three dimensions.

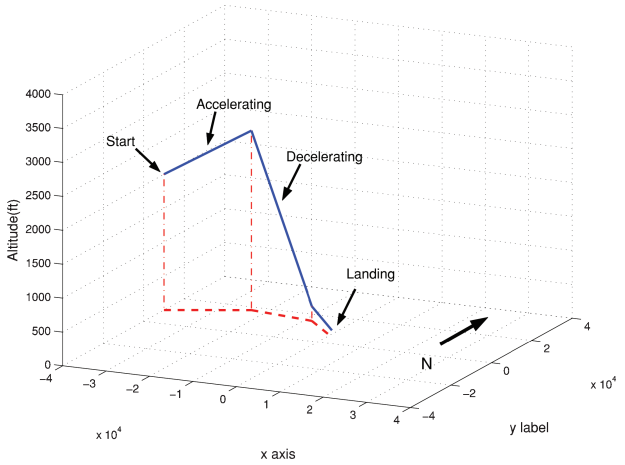

a) Optimal trajectory without population model ($W_k = 1.0$)

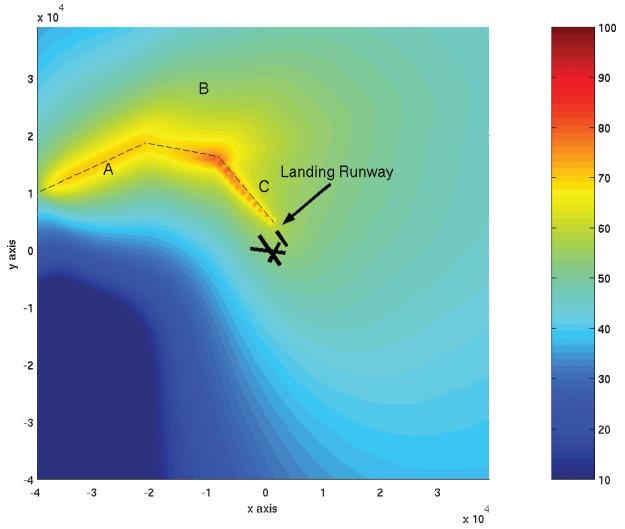

b) BVI SEL distribution ($W_k = 1.0$)

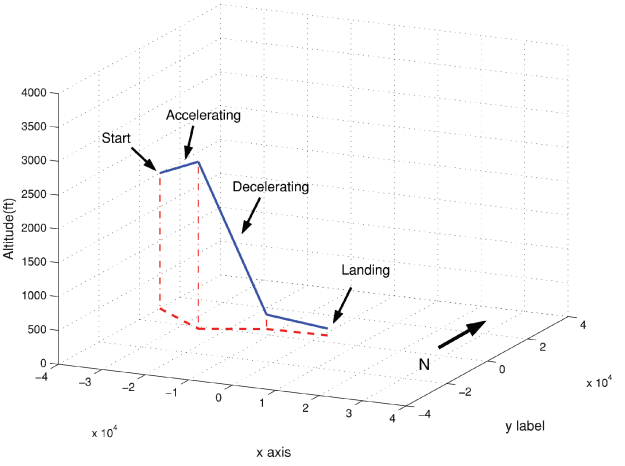

c) Optimal trajectory with population model

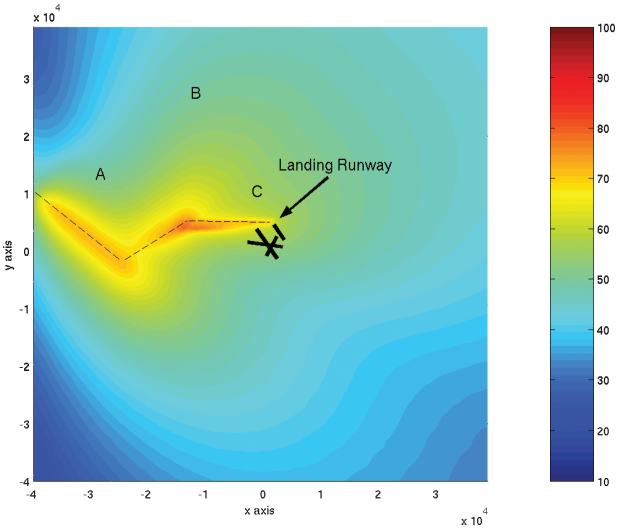

d) BVI SEL distribution

Fig. 16 Effects of population density on noise-optimal solution.

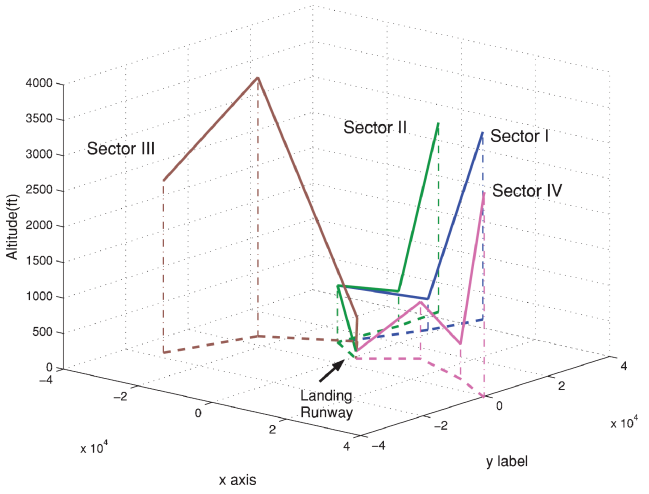

a) Optimal trajectories

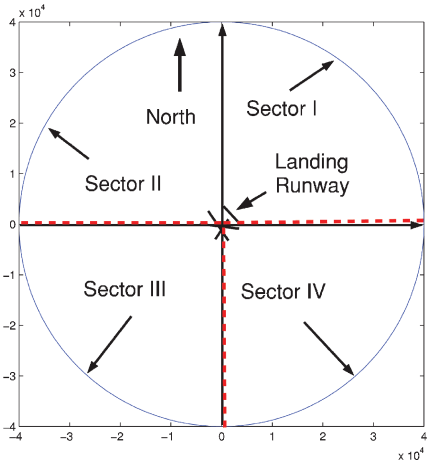

b) Sector definition

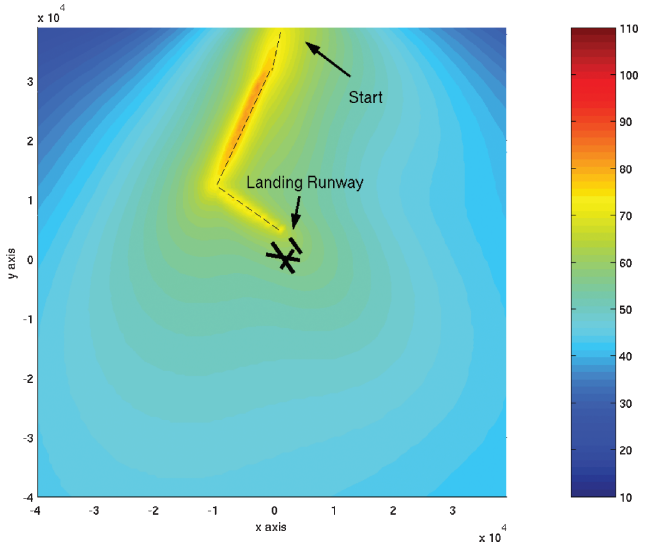

c) Sector I

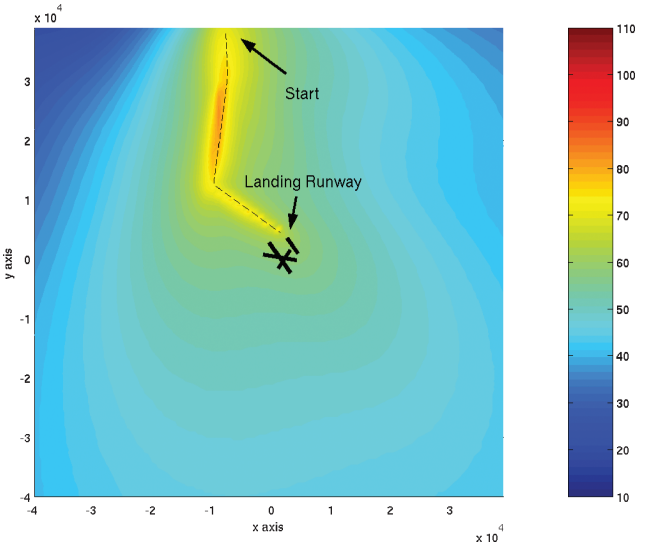

d) Sector II

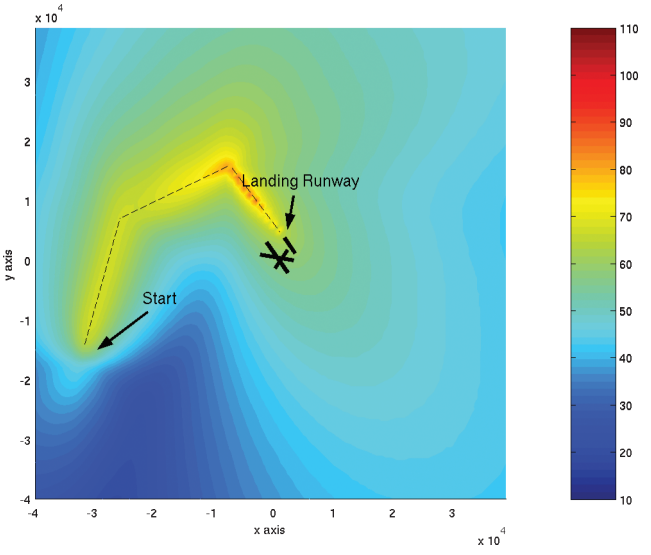

e) Sector III

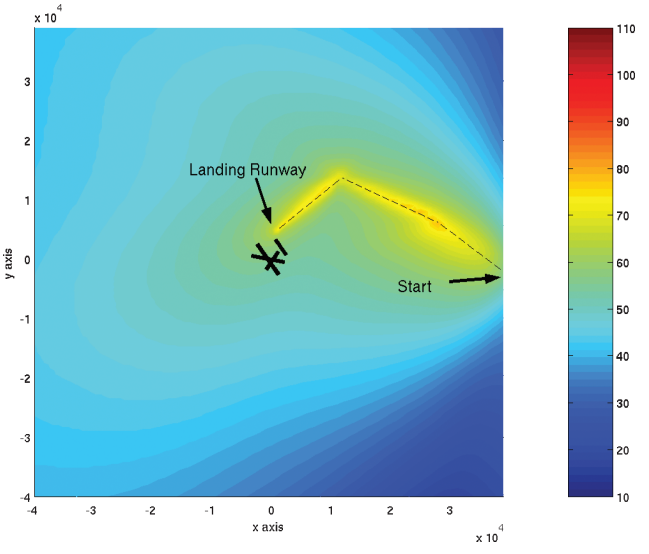

f) Sector IV

Fig. 17 Path shape and BVI SEL distribution for traffic from different sectors.

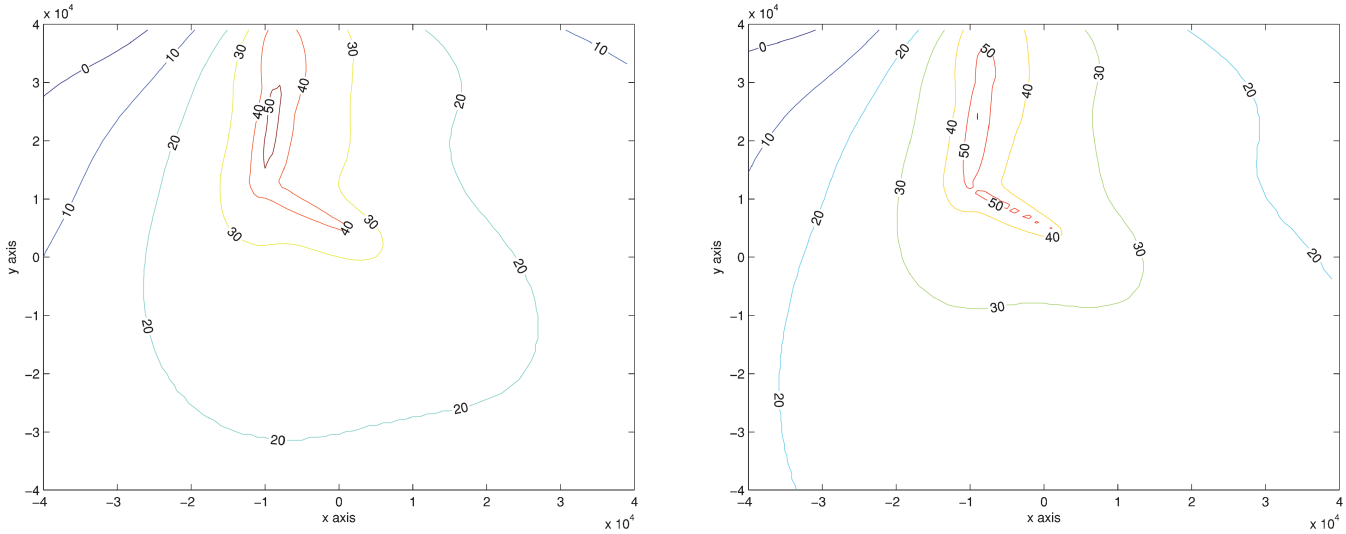

a) 100 flights/day **b) 300 flights/day**

Fig. 18 DNL distributions with solution of sector II.

With a rotorcraft as a RIA, numerous alternative landing sites at BWI could be identified in future work, and this optimization tool can assist with the selection of such a vertiport by defining candidate SNI RIA traffic procedures and their impact on the surrounding population.

V. Conclusions

This paper has presented models and methods to build optimal segmented noise abatement procedures (NAPs) for runway-independent aircraft (RIA). These trajectories will enable simultaneous, noninterfering (SNI) operations because airspace occupied by fixed-wing traffic is strictly excluded from proposed RIA routes. Taking as input a landing site, airport area population and flight track data and RIA performance constraints and noise model, our discrete optimization tool builds a k-ary tree to represent trajectory segments and uses an efficient Dijkstra's search algorithm to identify the globally optimal segmented solution. As a practical case study, SNI RIA routes have been computed for an AH-1 rotorcraft on approach to runway 15L at BWI airport, a viable landing choice for both VTOL and ESTOL vehicles. Population and flight track data for BWI are incorporated along with a model of AH-1 rotorcraft performance constraints and blade-vortex interaction (BVI), the dominant noise source during approach to landing.

Perhaps the most significant result from this study is that true SNI trajectories do exist without alteration to existing fixed-wing traffic patterns. In fact, SNI solutions can be found from all approach directions to BWI 15L, albeit at nonnegligible cost increase when a fixed-wing approach/departure corridor must be avoided. For the AH-1, optimal trajectories are driven to the maximum allowed climb/descent flight-path angles to minimize BVI. As might be expected, inclusion of population density guides the optimal flight track away from highly populated areas and reserves any higher-BVI configuration (e.g., shallow descent) for the final approach segment near the runway threshold, where population is sparse. The optimizer is able to reduce noise with an increased number of flight segments, but the tradeoff between NAP simplicity and noise level will likely favor a trajectory with few segments because, for our test cases, further noise reduction is minimal once three or more flight segments are included in the NAP.

The segmented trajectory optimization algorithm, BWI population/traffic models, and data interfaces are general for any RIA modeled at any level of fidelity. However, a number of simplifications were made in our analysis that will require extension in future work. Perhaps the most significant assumption is that transitions between trim states do not appreciably affect solution cost. Heading changes between flight segments will alter both noise magnitude and direction of propagation. Additionally, when the AH-1 transitions from a steep climb to a steep descent, the wake must pass briefly through the rotor disk, creating a short-term but high-magnitude BVI. Such transitions can be accurately modeled without modification to the segmented route search space by adding their effects on integrated path cost. The effects of wind can be modeled similarly, potentially resulting in a family of NAPs customized to different steady/gust wind conditions.

To perform optimization of AH-1 departure NAPs and further improve noise predictions for arrivals, the noise model must be expanded to include, as a minimum, tail rotor and engine noise. The current BVI model (Q-SAM) is being expanded for application to nonsteady flight and nonnegligible wind conditions and is also expected to be integrated into the standard integrated noise model (INM) noise predication software package that already includes extensive models for engine noise. As alternative RIA performance and noise models are developed, we will expand our models to include both VTOL and ESTOL vehicle classes. It is expected that mixed-fleet RIA operations will require approach/departure procedures customized at least to vehicle class, providing new challenges for air traffic operations accustomed to fixed queues of aircraft following roughly the same approach/departure paths. However, so long as the RIA routes remain SNI and ground operations are appropriately augmented to support RIA once on the ground, regular fixed-wing operations should not be impacted. The results of an optimization procedure such as that proposed in this work provide a guide for airport designers, and utilities will always be included to facilitate route customization and cost tradeoffs. The realization of RIA as a viable transportation option will be driven by congestion and will be made possible only with designs for aircraft and operational procedures that are economical, reliable, and accepted by passengers.

Acknowledgments

This research was supported by the National Rotorcraft Technology Center under the Rotorcraft Center of Excellence Program. The authors would like to thank Arnat Vale for providing information on BWI airport operations and the flight track data that enabled our development of SNI approach paths. We also are very grateful to Fred Schmitz, Ben Sim, and Gaurav Gopalan who provided us with the AH-1 BVI noise data and patiently guided us through its use.

References

[1]Newman, D., and Wilkins, R., "Rotorcraft Integration into the Next Generation NAS," *Proceedings of the American Helicopter Society (AHS) 54th Annual Forum*, American Helicopter Society, Alexandria, VA, 1998.

[2]Atkins, E. M., and Xue, M., "Noise-Sensitive Final Approach Trajectory Optimization for Runway-Independent Aircraft," *Journal of Aerospace Computation, Information and Communication*, Vol. 1, July 2004, pp. 269–287.

[3]Clarke, J.-P., "Systems Analysis of Noise Abatement Procedures Enabled by Advanced Flight Guidance Technology," *Journal of Aircraft*, Vol. 37, No. 2, 2000, pp. 266–273.

[4]Elmer, K., Wat, J., Shivashankara, B., Clarke, J.-P., Tong, K., Brown, J., and Warren, A., "Community Noise Reduction Using Continuous Descent Approach: A Demonstration Flight Test at Louisville," *Proceedings of the 9th AIAA/CEAS Aeroacoustics Conference and Exhibit*, AIAA, Reston, VA, 2003.

[5]Visser, H. G., and Wijnen, R. A. A., "Optimization of Noise Abatement Arrival Trajectories," AIAA Paper 2001-4222, Aug. 2001.

[6]Visser, H. G., and Wijnen, R. A. A., "Optimization of Noise Abatement Departure Trajectories," *Journal of Aircraft*, Vol. 38, No. 4, 2001, pp. 620–627.

[7]Vormer, F. J., Mulder, M., van Paassen, M. M., and Mulder, J. A., "Design and Preliminary Evaluation of Segment-based Routing Methodology," *Proceedings of Guidance, Navigation, and Control Conference*, AIAA, Reston, VA, 2002.

[8]Gopalan, G., Schmitz, F. H., and Sim, B. W., "Flight Path Management and Control Methodology to Reduce Helicopter Blade-Vortex (BVI) Noise," *Proceedings of the American Helicopter Society (AHS) Vertical Lift Aircraft Design Conference*, American Helicopter Society, Alexandria, VA, 2000.

[9]Latombe, J. C., *Robot Motion Planning*, Kluwer, 1991, Chaps. 4–7.

[10]Ladd, A. M., and Kavraki, L. E., "Measure Theoretic Analysis of Probabilistic Path Planning," *Transactions on Robotics and Automation*, Vol. 20, No. 2, 2004, pp. 229–242.

[11]Cheng, P., Shen, Z., and LaValle, S. M., "RRT-based Trajectory Design for Autonomous Automobiles and Spacecraft," *Archives of Control Sciences*, Vol. 11, Nos. 3–4, 2001, pp. 167–194.

[12]Albus, J., DeClaris, N., Lacaze, A., and Meystel, A., "Neural Network Based Planner/Learner for Control Systems," *Proceedings of the 1997 International Conference on Intelligent Systems and Semiotics*, 1997, pp. 75–81.

[13]Bersekas, D., and Gallager, R., *Data Networks*, Prentice–Hall, 1992, Chap. 5.

[14]Russell, S., and Norvig, P., *Artificial Intelligence: a Modern Approach*, Prentice Hall Series, NJ, 1995, Chaps. 3–4.

[15]Dean, T., Kaelbling, L. P., Kirman, J., and Nicholson, A., "Planning Under Time Constraints in Stochastic Domains," *Artificial Intelligence*, Vol. 76, Nos. 1–2, 1995, pp. 35–74.

[16]Johnson, W., *Helicopter Theory*, Dover, New York, 1994, Chap. 6.

[17]"Quarterly Noise Report—Fourth Quarter 2002," Airport Noise and Abatement Office, Maryland Aviation Administration, 2003.